

**Crossing the superfluid-supersolid transition of an elongated dipolar condensate**Aitor Alaña <sup>1,2</sup> Nicolò Antolini <sup>3,4</sup> Giulio Biagioni <sup>3,5</sup> Iñigo L. Egusquiza <sup>1,2</sup> and Michele Modugno <sup>1,2,6</sup><sup>1</sup>*Department of Physics, University of the Basque Country UPV/EHU, 48080 Bilbao, Spain*<sup>2</sup>*EHU Quantum Center, University of the Basque Country UPV/EHU, 48940 Leioa, Biscay, Spain*<sup>3</sup>*Consiglio Nazionale delle Ricerche-INO, Sede di Pisa, 56124 Pisa, Italy*<sup>4</sup>*CNR-INO, Sede di Pisa, 56124 Pisa, Italy*<sup>5</sup>*Department of Physics and Astronomy, University of Florence, 50019 Sesto Fiorentino, Italy*<sup>6</sup>*IKERBASQUE, Basque Foundation for Science, 48013 Bilbao, Spain*

(Received 15 July 2022; accepted 27 September 2022; published 14 October 2022)

We provide a theoretical characterization of the dynamical crossing of the superfluid-supersolid phase transition for a dipolar condensate confined in an elongated trap, as observed in the recent experiment by Biagioni *et al.* [G. Biagioni, N. Antolini, A. Alaña, M. Modugno, A. Fioretti, C. Gabbanini, L. Tanzi, and G. Modugno, *Phys. Rev. X* **12**, 021019 (2022)]. By means of the extended Gross-Pitaevskii theory, which includes the Lee-Huang-Yang quantum fluctuation correction, we first analyze the ground-state configurations of the system as a function of the interparticle scattering length, for both trap configurations employed in the experiment. Then, we discuss the effects of the ramp velocity, by which the scattering length is tuned across the transition, on the collective excitations of the system in both the superfluid and supersolid phases. We find that, when the transverse confinement is sufficiently strong and the transition has a smooth (continuous) character, the system essentially displays a (quasi) one-dimensional behavior, its excitation dynamics being dominated by the axial breathing modes. Instead, for shallower transverse trapping, when the transition becomes discontinuous, the collective excitations of the supersolid display a coupling with the transverse modes, signaling the onset of a dimensional crossover.

DOI: [10.1103/PhysRevA.106.043313](https://doi.org/10.1103/PhysRevA.106.043313)**I. INTRODUCTION**

Supersolids (SSs) are an exotic phase of matter combining superfluid (SF) properties (phase coherence and frictionless flow [1,2]) with the translational symmetry breaking that characterizes crystalline structures [3–6]. First predicted in the 1950s [7,8], supersolids have gained the interest of the scientific community as a consequence of their recent experimental realizations in dipolar condensates [9–17] and in other ultracold atomic systems [18–20]. In particular, Ref. [21] has recently reported the experimental investigation of the superfluid-supersolid quantum phase transition in an elongated dipolar condensate, driven by tuning the interparticle interactions (by means of Feshbach resonances). Remarkably, it has been shown that the character of the transition can be changed from continuous to discontinuous simply by tuning the transverse confinement (or the atom number), therefore providing a dimensional crossover between second-order transitions in one dimension [22,23] and first-order transitions in two dimensions [9,10,12,24–26].

In the present paper we provide a complementary theoretical characterization of the equilibrium and dynamical properties of the dipolar condensate in the two trap configurations,  $V_C$  and  $V_D$ , employed in the experiment of Ref. [21]. This analysis is carried out within the standard framework of the extended Gross-Pitaevskii (GP) theory [27], including both contact and dipolar interactions [28], as well as the

Lee-Huang-Yang (LHY) quantum correction [29]. We first consider the equilibrium properties of this system and we show that the trap characterized by a tighter transverse confinement ( $V_C$ ) presents a smooth, i.e., continuous, transition between the superfluid and supersolid phases, whereas for shallower trapping potentials ( $V_D$ ) a discontinuous character clearly shows up. Then, we thoroughly discuss how the velocity of the ramp employed to experimentally tune the  $s$ -wave scattering length across the transition affects the dynamical response of the system, commenting also on the role of the formation time of the supersolid. Remarkably, we find that—when the system enters the supersolid phase—the collective modes in the two traps present distinctive behaviors: in the trap  $V_C$ , where the system can be considered effectively quasi-one dimensional (1D), the excitation dynamics is dominated by the axial breathing modes; instead, in the trap  $V_D$ , the axial excitations of the supersolid display a clear coupling to the collective transverse modes. This provides a signature of the onset of a dimensional crossover, in agreement with the discussion in Ref. [21].

The paper is organized as follows. In Sec. II we introduce the system parameters and the general framework of the extended Gross-Pitaevskii theory for dipolar condensates. Then, in Sec. III we analyze the equilibrium properties of the condensate in the two trap configurations,  $V_C$  and  $V_D$ , and we characterize the corresponding superfluid-supersolid transition as a function of the  $s$ -wave scattering length.

Section IV is instead devoted to the dynamical crossing of the transition. We first address, in Sec. IV A, the effect of the ramp velocity and then, in Sec. IV B, we discuss how the formation time of the supersolid affects the crossing of the transition. Finally, in Sec. IV C we examine the collective oscillations of the system that arise due to the excess of energy acquired during the ramp across the transition, in both the supersolid and superfluid phases. Concluding remarks are presented in Sec. V.

## II. SYSTEM

We consider the typical experimental configuration of Ref. [21]. A dipolar condensate composed by  $N = 3 \times 10^4$  magnetic atoms of  $^{162}\text{Dy}$ —with tunable  $s$ -wave scattering length  $a_s$  and dipolar length  $a_{dd} = 130a_0$  ( $a_0$  being the Bohr radius)—is trapped by a harmonic potential with frequencies  $\omega = 2\pi \times (\nu_x, \nu_y, \nu_z)$ . As in the experiment, we consider two different trap configurations, namely,  $\omega_C = 2\pi \times (15, 101, 94)$  Hz and  $\omega_D = 2\pi \times (20, 67, 102)$  Hz, where the labels  $C$  and  $D$  refer to the continuous and discontinuous character of the transition (see Sec. III), respectively, in line with the notations employed in Ref. [21]. Accordingly, we indicate the corresponding harmonic potentials as  $V_C$  and  $V_D$ .

This system can be described in terms of a generalized GP theory including dipolar interactions [28] and the Lee-Huang-Yang correction accounting for quantum fluctuations (within the local-density approximation) [29]. The energy functional can be written as  $E = E_{\text{GP}} + E_{dd} + E_{\text{LHY}}$  with

$$\begin{aligned} E_{\text{GP}} &= \int \left[ \frac{\hbar^2}{2m} |\nabla \psi(\mathbf{r})|^2 + V_{C/D}(\mathbf{r})n(\mathbf{r}) + \frac{g}{2}n^2(\mathbf{r}) \right] d\mathbf{r}, \\ E_{dd} &= \frac{C_{dd}}{2} \iint n(\mathbf{r})V_{dd}(\mathbf{r} - \mathbf{r}')n(\mathbf{r}')d\mathbf{r}d\mathbf{r}', \\ E_{\text{LHY}} &= g_{\text{LHY}} \int n^{5/2}(\mathbf{r})d\mathbf{r}, \end{aligned} \quad (1)$$

where  $E_{\text{GP}} = E_k + E_{ho} + E_{\text{int}}$  is the standard GP energy functional including the kinetic, potential, and contact interaction terms,  $V(\mathbf{r}) = (m/2) \sum_{\alpha=x,y,z} \omega_\alpha^2 r_\alpha^2$  is the harmonic trapping potential,  $n(\mathbf{r}) = |\psi(\mathbf{r})|^2$  represents the condensate density (normalized to the total number of atoms  $N$ ),  $g = 4\pi\hbar^2 a_s/m$  is the contact interaction strength,  $V_{dd}(\mathbf{r}) = (1 - 3\cos^2\theta)/(4\pi r^3)$  is the (bare) dipole-dipole potential,  $C_{dd} \equiv \mu_0\mu^2$  is its strength,  $\mu$  is the modulus of the dipole moment  $\boldsymbol{\mu}$ ,  $\mathbf{r}$  is the distance between the dipoles, and  $\theta$  is the angle between the vector  $\mathbf{r}$  and the dipole axis,  $\cos\theta = \boldsymbol{\mu} \cdot \mathbf{r}/(\mu r)$ . As in Ref. [21] we consider the magnetic dipoles to be aligned along the  $z$  direction by a magnetic field  $\mathbf{B}$ . Finally, the LHY correction is obtained from the expression for homogeneous three-dimensional dipolar condensates under the local-density approximation [29,30]. The LHY coefficient is  $g_{\text{LHY}} = 256\sqrt{\pi}\hbar^2 a_s^{5/2}/(15m)(1 + 3\epsilon_{dd}^2/2)$ , with  $\epsilon_{dd} = \mu_0\mu^2 N/(3g)$ .

## III. GROUND STATE

We compute the ground state of the system by minimizing numerically the energy functional  $E[\psi]$  by means of a conju-

gate algorithm (see, e.g., Refs. [31,32]). In the numerical code the double integral appearing in Eq. (1) is mapped into Fourier space where it can be conveniently computed by means of fast Fourier-transform (FFT) algorithms, after regularization [28,33]. The behavior of the ground-state energy for the two potentials is shown in Fig. 1 as a function of the  $s$ -wave scattering length  $a_s$ , in the range  $a_s \in [90, 96]a_0$ , along with some representative images of the density distributions in the SS and SF phases [34]. Notice that in the supersolid phase both traps  $V_C$  and  $V_D$  exhibit two almost degenerate configurations, characterized by either a maximum or a minimum at the center of the trap [35]. These two states are those that—for symmetry reasons—survive in the presence of the trap among the infinite equivalent configurations that would be possible in a (infinite) uniform system [36].

Let us start by considering the case of the potential  $V_C$  (characterized by the tighter confinement along the  $y$  direction), shown in the left panel of Fig. 1. For this trap, the transition takes place at  $a_s^c \simeq 94.4a_0$  and it exhibits a continuous behavior: the superfluid and the supersolid states morph continuously one into the other, as do their energies [see the inset of Fig. 1 (left)]. The critical point can be identified, for instance, by the slope change in the first derivative of the energy with respect to the  $s$ -wave scattering length (see Fig. 2). The continuity of  $\partial E/\partial a_s$  at the critical point confirms the continuous character of the transition in this case (within the numerical precision).

In the case of the potential  $V_D$ , which is characterized by a weaker transverse confinement, the transition takes place at lower value of the scattering length, namely,  $a_s^c \simeq 92.4a_0$ . Remarkably, in this case the two SS states manifest a different behavior in the vicinity of the transition [see the inset of Fig. 1 (right panel)]. In particular, the configuration with a maximum at the trap center is the one with lower energy at the boundary with the SF phase, so that  $a_s^c$  is actually defined by the crossing of the energy of such a state with that of the SF state. The transition clearly exhibits a discontinuous jump in the first derivative of the energy with respect to the  $s$ -wave scattering length (see Fig. 2). As discussed in Ref. [21], this discontinuous behavior of the SF-SS transition is reminiscent of that expected for trapped supersolids with two-dimensional (2D) lattice structures [37–40], and it is due to the fact that even in the case of a single row supersolid the background density may exhibit a triangular structure. Even if not visible in the snapshots in Fig. 1, this structure is enhanced when the system is out of equilibrium. Indeed, a clear 2D modulation of the background density can be observed during the dynamics of the supersolid discussed in the following section.

## IV. DYNAMICAL STUDY OF THE TRANSITION

We now turn to the dynamical study of the phase transition, following a protocol similar to the one employed in the experiment of Ref. [21]: The system is initially prepared in a stationary superfluid or supersolid state, at a certain scattering length  $a_s^i$ , and then the value of  $a_s$  is tuned along a linear ramp with constant velocity  $da_s/dt \equiv v_a$  towards a final value  $a_s^f$ , in the other phase. The ramp scheme and the simulation timing are shown in Fig. 3. For conceptual clarity, here we consider  $a_s^i$  and  $a_s^f$  to be in specular position with respect to

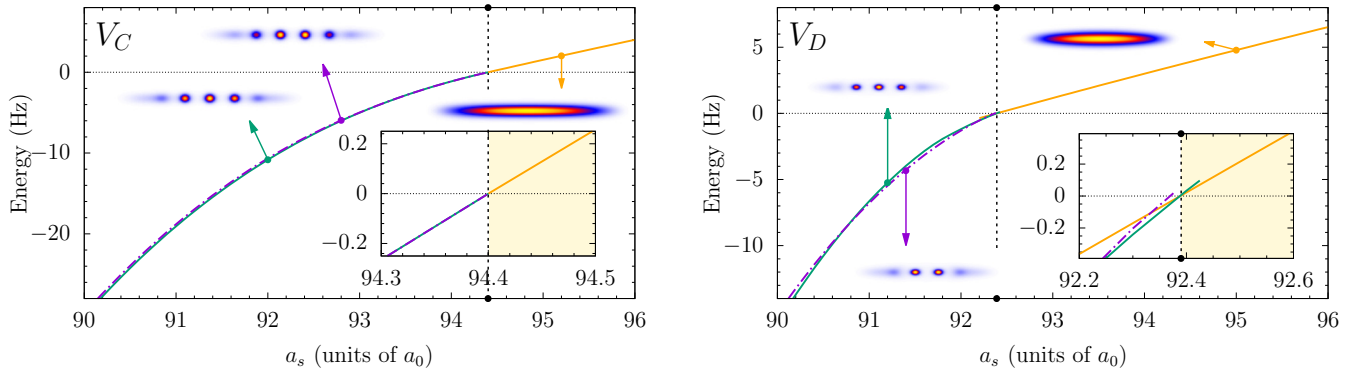


FIG. 1. Normalized energy,  $(E[a_s] - E[a_s^c])/h$  (where  $E[a_s^c]/h$  corresponds to 432.2 Hz for  $V_C$  and 476.7 Hz for  $V_D$ ), for the supersolid and superfluid density configurations, as a function of the contact scattering length  $a_s$ , for potentials  $V_C$  (left) and  $V_D$  (right). Typical density distributions (see text; in each plot the color scale is weighted by the density distribution) are indicated by the arrows (the colors of which match the color of the corresponding energy lines). The vertical dashed line represents the boundary between the supersolid and superfluid phases (on its left and right, respectively), at the critical scattering length  $a_s^c$ . The insets show the energy behavior in the vicinity of  $a_s^c$ .

the critical point  $a_s^c$ , namely,  $a_s^{i/f} = a_s^c \pm \delta a_s$ . In the following, we shall consider  $\delta a_s = 1.5a_0$  and three ramps with different velocities: (i) a “quench”,  $v_a = \infty$ ; (ii)  $v_a = 0.5 a_0/\text{ms}$ , which corresponds to the nominal velocity employed in the experiment [21] (and of the same order of that of Ref. [10]); and (iii)  $v_a = 0.05 a_0/\text{ms}$ , a lower velocity that allows for a quasiadiabatic crossing of the supersolid-superfluid transition in the trap  $V_C$  (see Sec. IV A), as discussed in Ref. [21]. This latter choice permits us to reproduce a scenario similar to that of the above-mentioned experiment, without having to introduce dissipation effects in the theoretical modeling (which are instead present in the experiment [21]) [41].

Therefore, in the following we shall restrict the discussion to the dissipationless scenario, obtained by solving the GP equation [2]

$$i\hbar\partial_t\psi = \delta E[\psi, \psi^*]/\delta\psi^*, \quad (2)$$

where the energy functional  $E[\psi, \psi^*]$  is the one in Eq. (1) [42]. Regarding the two supersolid configurations discussed in the previous section, we notice that during the dynamics across the SF-SS transition the system is likely to select spontaneously the configuration with a maximum at the center of the trap, so that we have used such a configuration also for the

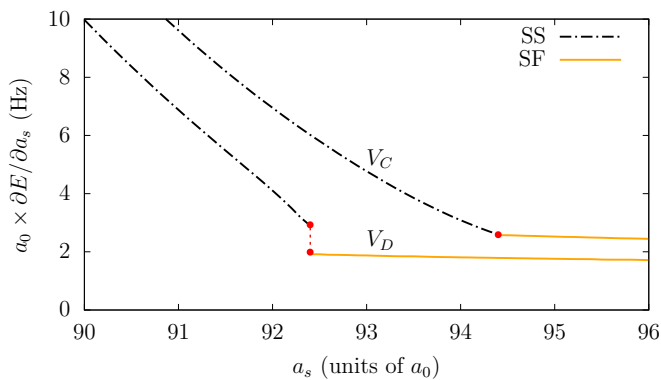


FIG. 2. Derivative of the total energy of the ground state for the two trap configurations,  $V_C$  and  $V_D$ . The latter exhibits a discontinuity (vertical dashed line) at the transition point (red dots).

initial state of the ramp in the opposite direction, for the sake of simplicity.

### A. Effect of the ramp

Let us now discuss how the system gets modified while varying the scattering length. In particular, we shall first consider how the different ramp velocities affect the energy of the system, and which is the final density distribution of the condensate at the end of each ramp (the dynamics following the end of the ramp will be discussed in Sec. IV C). This is shown in Figs. 4 and 5, for the traps  $V_C$  and  $V_D$ , respectively. In the top panel we show the behavior of the energy of the system as a function of the scattering length  $a_s(t)$  along the three ramps across the SF-SS transition (blue lines) and in the opposite direction, from SS to SF (red lines). In the case of the quench, the line is simply a guide to the eye that connects the initial and final value of the scattering length. The insets represent the initial configurations in the SF and SS phases. The density distributions obtained at the end of each ramp, namely, at  $t = t_R$ , are shown in panels (a)–(c) in Figs. 4 and 5

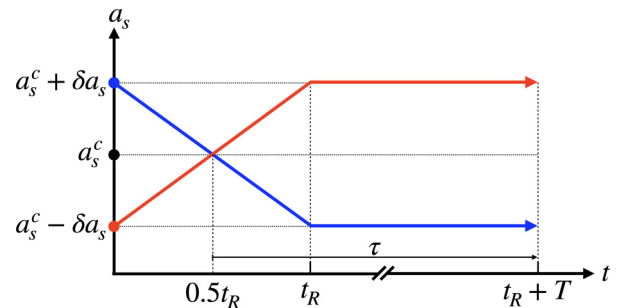


FIG. 3. Scheme of the ramp employed in the numerical simulations: the system is prepared in the ground state either in the superfluid or in the supersolid phase, at  $a_s^i = a_s^c \pm \delta a_s$ , and then the scattering length is varied along a linear ramp—during a time  $t_R \equiv 2\delta a_s/v_a$ —towards a final value in other phase,  $a_s^f = a_s^c \mp \delta a_s$ . Then, the system is kept at the final value  $a_s^f$  for a variable time  $T$ . The time spent in the SS or SF phase after crossing the critical value of the scattering length is indicated as  $\tau$  (see Sec. IV B).

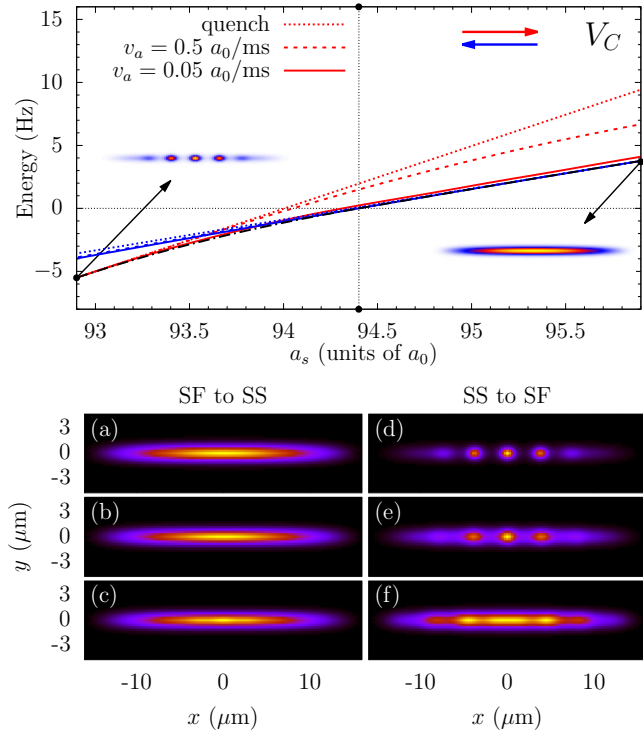


FIG. 4. Behavior of the system along the linear ramp across the SF-SS transition, for the trap  $V_C$ . Top: Behavior of the normalized energy of the system  $(E[a_s] - E_{gs}[a_s^c])/h$ , as a function of the scattering length  $a_s(t)$  during the ramp, for different ramp velocities (see legends) and directions (red, SS to SF; blue, SF to SS). The black dots represent the ground-state energy. (a–c) Density distribution at the end of the downward ramp from SF to SS, for (a) a quench ( $t_R = 0$  ms), (b)  $v_a = 0.5 a_0/\text{ms}$  ( $t_R = 6$  ms), and (c)  $v_a = 0.05 a_0/\text{ms}$  ( $t_R = 60$  ms). (d–f) The corresponding distributions after the upward ramp from SS to SF. Notice that the density distributions shown for the case of a quench in panels (a) and (d) correspond, by definition, to the initial density distribution at the beginning of the ramp (also shown as insets in the main panel). In each plot the color scale is weighted by the density distribution.

for the SF-SS transition and in panels (d)–(f) in Figs. 4 and 5 for the SS-SF transition.

It is interesting to notice that, when crossing the transition in the downward direction, from SF to SS, both the energy variation and the final density distribution are weakly affected by the ramp velocity. In the case of a quench, this has to be so because the system is “projected” instantaneously in the other quantum phase without changing its density distribution, so that in this case the final configurations exactly coincide with the initial ones. The case at  $v_a = 0.5 a_0/\text{ms}$  turns out to be almost equivalent to a quench (in contrast to what happens during the SS–SF transition; see below). Only in the case of the slowest ramp at  $v_a = 0.05 a_0/\text{ms}$  in the trap  $V_D$  can a slight modulation superimposed to the initial state be appreciated. The origin of this behavior has to do with the *formation time of the supersolid* (see, e.g., Ref. [10]), that will be discussed in Sec. IV B.

In the opposite direction, when crossing the SS to SF transition, the behavior is quite different: The energy grows linearly if the scattering length is quenched, while it follows

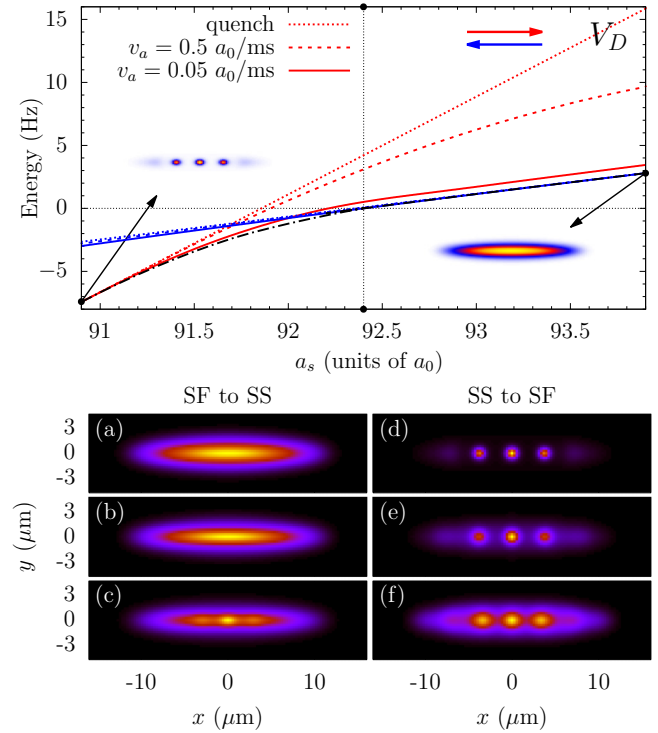


FIG. 5. Behavior of the system along the linear ramp across the SF-SS transition, for the trap  $V_D$ . The conventions and the quantities being plotted are the same as in Fig. 4.

the ground-state energy almost adiabatically if the scattering length is slowly varied (at  $v_a = 0.05 a_0/\text{ms}$ ). In addition, it is evident both from the energy behavior and from the final configuration in Fig. 4(f) that for the trap  $V_C$  such a ramp is sufficiently slow to bring the SS state close to the SF ground state, with a small excitation energy embedded in a density deformation that is reminiscent of the initial state. Remarkably, such a deformation is significantly larger in trap  $V_D$  [compare Figs. 4(f) and 5(f)]. Moreover, the residual energy on the superfluid side is larger in trap  $V_D$  than in trap  $V_C$  for each of the three ramps (see also the discussion in Ref. [21]). These observations are consistent with the continuous or discontinuous character of the transition in the two cases.

In order to get further insight on the behavior of the total energy along the ramp it is convenient to rewrite the energy functional (1) in the following form, which makes apparent for which terms the dependence on  $a_s$  is explicit:

$$E[\psi; a_s] = E_k[\psi] + E_{ho}[n] + a_s \mathcal{E}^{\text{int}}[n] + E_{dd}[n] + a_s^{5/2} \left[ 1 + \frac{3}{2} \left( \frac{a_{dd}}{a_s} \right)^2 \right] \mathcal{E}^{\text{LHY}}[n], \quad (3)$$

with  $\mathcal{E}^{\text{int}}[n]$  and  $\mathcal{E}^{\text{LHY}}[n]$  functionals that depend on the density only. Thus, the dependence on the scattering length is explicit for the mean-field interaction energy and the LHY correction, whereas all the other terms depend on  $a_s$  only indirectly, through the condensate density (and in the case of the kinetic term also through the phase of the wave function).

The behavior of the system during the ramp across the transition is therefore characterized by two timescales: The one associated to the variations of the scattering length,



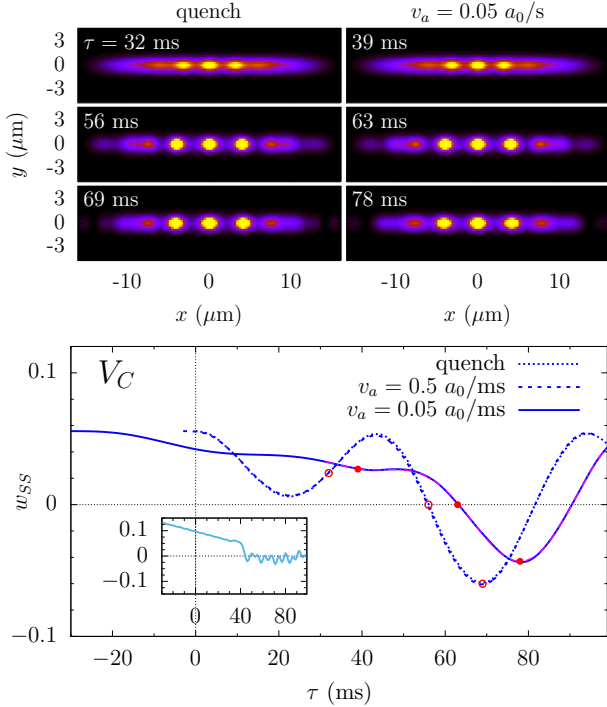


FIG. 6. Dynamical behavior of the system in the SS phase, for the trap  $V_C$ . The time  $\tau = 0$  corresponds to the crossing of the SF-SS transition. Top: Density distribution at selected times (see labels) for a quench (left) and for  $v_a = 0.05 a_0/ms$  (right). All densities are saturated at the same level. The case at  $v_a = 0.5 a_0/ms$ , not shown, is very similar to the quench. The panels in the top row correspond to the time at which the supersolid structure starts to emerge clearly,  $\tau \approx 30$ – $40$  ms. Bottom: Evolution of the (dimensionless) axial width  $w_{SS}(\tau)$  [see Eq. (4)], for the three ramp velocities considered here. The empty/solid red dots corresponds to the density distributions shown in the top panels. The (magenta) dot-dashed line represents a sinusoidal fit with two frequencies,  $\nu_+ \simeq 24.0$  (Hz) and  $\nu_- \simeq 13.9$  (Hz), accounting for the doubling of the axial breathing mode of a supersolid (see text). The inset shows the behavior of the transverse width  $w_{SS}(\tau)$  along the direction  $y$  (for  $v_a = 0.05 a_0/ms$ ).

controlled by the ramp duration  $t_R = 2\delta a_s/v_a$ , and the timescale required for variations in the condensate density to appear. Remarkably, the latter strongly depends on the phase of the system. In the SS phase, the emergence of the crystalline order of a supersolid is characterized by a minimal formation time  $\tau_{SS} \approx 30$  ms, as we shall see in the following section (see also Ref. [10]). As a consequence, in the present setup the system cannot undergo significant density modifications during the SF-SS ramp (not even in the case of the slowest ramp), such that in this case the energy variations are dictated only by the explicit dependence on  $a_s$ . In particular, by considering that  $E^{LH} \ll E^{int}$ , in this case the energy variation can be written as  $\delta E \simeq \delta a_s \mathcal{E}^{int}[n]$  [see Eq. (3)], which corresponds to linear behavior shown in Figs. 4 and 5.

When going from SS to SF the scenario is quite different. In fact, when the scattering length is increased during the upward ramp, the system can gradually relax the initial supersolid profile into a smoother one, suppressing the crystalline order. In the SF phase the relevant timescale is the one characterizing the collective excitations of the condensate,

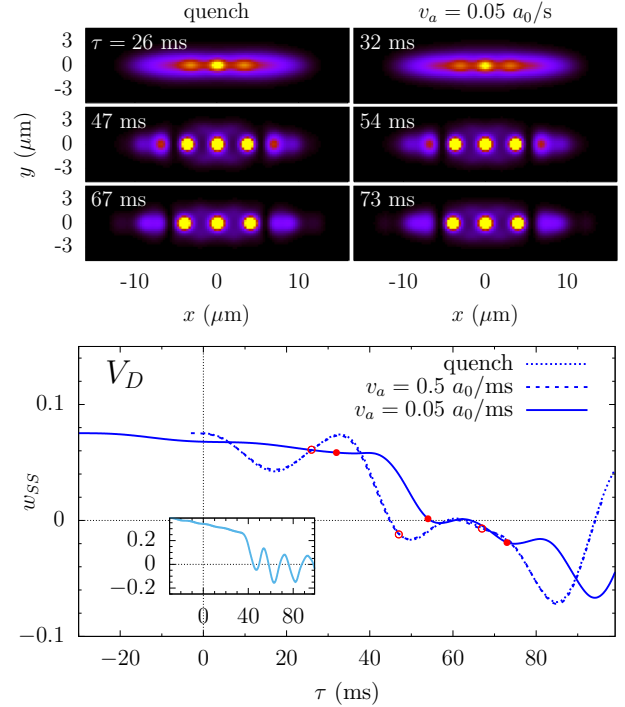


FIG. 7. Dynamical behavior of the system once it has entered the SS phase, for the trap  $V_D$ . The quantities plotted are the same as in Fig. 6. Notice the appearance of a two-dimensional structure during the evolution (second and third row of panels), associated to the onset of a transverse oscillation mode shown in the inset (see text). It is also worth noticing that in this trap the supersolid starts to form slightly earlier than in Fig. 6, at  $\tau \approx 25$ – $30$  ms (see the top panels).

which is of the order of  $\tau_0/4$ , with  $\tau_0$  being the oscillation period of the main excitation mode. In the present case, the dynamics is dominated by the axial breathing mode [12], and the associated timescale is of the order of few milliseconds (see Sec. IV B) [43]. This explains the different behavior displayed by the three ramps. Notice that for the case of the quench the same argument of the SF to SS transition holds,  $\delta E \simeq \delta a_s \mathcal{E}^{int}[n]$ . More interesting is the behavior that characterizes the ramp at  $v_a = 0.05 a_0/ms$ : though the top panels in Figs. 4 and 5 may suggest that during the upward ramp the system evolves almost adiabatically in both traps  $V_D$  and  $V_C$ , the fact that the density distributions at the end of the ramp look quite different [see Figs. 4(f) and 5(f)] provides instead a signature that the two systems behave differently at the SS-SF transition, with only the one in the trap  $V_C$  displaying a (quasi) adiabatic behavior.

### B. Formation time of the supersolid

We now turn to the discussion of the formation time required for the supersolid to emerge after the system has been driven through the SF-SS transition. For convenience, here we introduce the time coordinate  $\tau \equiv t - t_R/2$ , that denotes the time elapsed from the crossing of the SF-SS transition (see Fig. 3).

In the case of the trap  $V_C$ , we find that the supersolid structure starts to develop at  $\tau_{SS}^C \approx 30$ – $40$  ms (see the top row of Fig. 6). Instead, the trap  $V_D$  is characterized by shorter

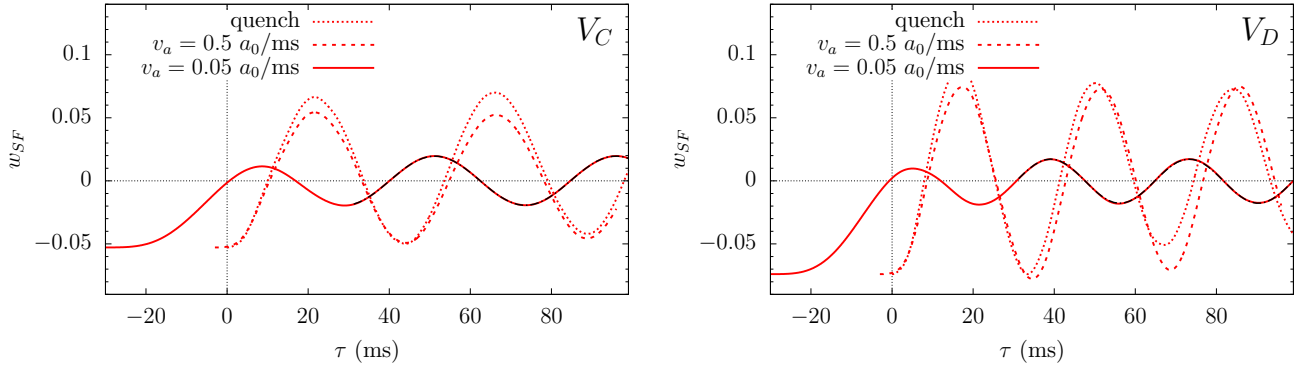


FIG. 8. Evolution of the (dimensionless) normalized relative width  $w_{\text{SF}}(\tau)$  defined in Eq. (4), for the potential  $V_C$  (left) and  $V_D$  (right). The black dot-dashed line superimposed to the line at  $v_a = 0.05a_0/\text{ms}$  from the end of the ramp at  $\tau \geq 30$  ms represents a sinusoidal fit of the form  $A \sin(2\pi \nu t + \theta) + B$ . The fit returns  $\nu_D \simeq 29.3$  (Hz) and  $\nu_C \simeq 22.7$  (Hz), corresponding to the axial breathing mode (see text).

formation times,  $\tau_{\text{SS}}^D \approx 25\text{--}30$  ms (see Fig. 7). By accident, this formation time is of the order of  $t_R/2$  for the ramp at  $v_a = 0.05a_0/\text{ms}$ , and this explains why in this case the supersolid pattern already emerges at the end of the ramp [see Fig. 5(c)]. Notice that the formation times observed experimentally in Ref. [21] are shorter than those we find from the present numerical analysis, likely due to finite temperature effects and three-body losses (see also Refs. [10,44]).

Remarkably, the figures above also show that  $\tau_{\text{SS}}$  not only depends on the trap configuration, but also on the ramp velocity. Indeed, as discussed in Ref. [10], longer formation times are associated with a lower-energy difference between the initial superfluid configuration (at  $\tau = 0$ ) and the target equilibrium supersolid state. In the case of a quench this energy difference is fixed by the final value  $a_s^f$  of the scattering length, namely,  $\Delta E \equiv E_{\text{SF}}[a_s^f] - E_{\text{SS}}[a_s^f]$ , as the system is projected instantaneously from  $a_s^i$  to  $a_s^f$ . Instead, in the case of a linear ramp the system spends some time in passing from  $a_s^c$  to  $a_s^f$  so that, before reaching the final value of the scattering length, it has to cross a region where the energy gap between the SF and SS branches is smaller (see Fig. 4). This qualitatively explains the slight delay observed. Regarding the difference between the traps  $V_C$  and  $V_D$ , by comparing Figs. 4 and 5 it is evident that the latter is characterized by a larger gap, which therefore corresponds to a shorter formation time according to the above argument.

### C. Collective oscillations

Once the system has entered the new phase, either SS or SF, the excitation energy acquired during the ramp eventually drives the system into collective oscillations. In the present case, since the phase transition mainly affects the density distribution along the axial direction of the trap, the major contribution comes from the so-called axial breathing mode [12]. The latter can be conveniently characterized by considering the width along the  $x$  direction, which corresponds to the axial direction of the supersolid. In order to do so, we define a normalized relative width as

$$w_\alpha(t) \equiv [\sigma_x(t) - \sigma_{x\alpha}^{\text{eq}}] / \sigma_{x\alpha}^{\text{eq}}, \quad (4)$$

where  $\sigma_x^2(t) \equiv \langle x^2 \rangle = (1/N) \int x^2 n(\mathbf{r}, t) d\mathbf{r}$ ,  $\alpha$  indicates the SF and SS states, and  $\sigma_{x\alpha}^{\text{eq}}$  indicates the corresponding equilibrium widths at  $a_s^c \pm \delta a_s$ , respectively. In the following, we shall consider especially the behavior of the width as a function of the time  $\tau$  elapsed from the crossing of the SF-SS transition, namely,  $w_\alpha(\tau)$ . This quantity is shown in the bottom panels of Figs. 6 and 7 for the SS case, and in Fig. 8 for the SF case. Overall, the behavior of  $w_\alpha(\tau)$  provides an additional characterization of the (non)adiabaticity of the various ramps and of the character of the transition for the two trap configurations.

Let us first consider the SS case, in Figs. 6 and 7. First of all, we notice that the ramp at  $v_a = 0.5 a_0/\text{ms}$ , corresponding to the nominal value employed in the experimental protocol of Ref. [21], is almost indistinguishable from a quench. Instead, the slowest ramp at  $v_a = 0.05 a_0/\text{ms}$  presents a distinctive feature in the fact that the value of the width decreases gradually along the ramp,  $-30 < \tau < 30$  ms, indicating that the system is able to smoothly adjust its shape to the changing value of the scattering length, from  $a_s^i$  to  $a_s^f$ .

As discussed in Ref. [12], the excitation dynamics of an elongated supersolid is characterized by a *doubling* of the axial breathing mode of a dipolar condensate (in the SF regime; see below). The two modes that appear in the SS phase are associated to the deformation of the supersolid lattice structure, namely, its amplitude and spacing. The former is dominated by the higher-frequency mode, and the latter is dominated by the lower-frequency one. In the case of the trap  $V_C$  we observe indeed a beating of two frequencies (see Fig. 6) that we fit with a sinusoidal function of the form  $A_+ \sin(2\pi \nu_+ t + \theta_+) + A_- \sin(2\pi \nu_- t + \theta_-) + B$  (see the magenta dot-dashed lines in the figure). The fit of the curve at  $v_a = 0.05 a_0/\text{ms}$  returns  $(\nu_+/\nu_x)_C \simeq 1.6$  and  $(\nu_-/\nu_x)_C \simeq 0.93$ , which is consistent with the picture provided in Ref. [12] (here  $\epsilon_{dd}^C = 1.39$ ) [45]. A similar result is obtained from the fit of the other two lines. In the transverse directions we do not see instead any significant oscillation, as one can observe from the behavior of transverse width along the  $y$  direction shown in the inset. In the figure we also show a few snapshots of the density distribution, at selected times: when the supersolid structure starts to emerge clearly (top row, discussed previously), at  $w_{\text{SS}}(\tau) = 0$  (middle row), and when  $w_{\text{SS}}(\tau)$  first reaches a minimum of the oscillation (bottom row). These snapshots well represent

the qualitative behavior along the whole dynamics considered here [also when  $w_{SS}(\tau)$  gets to an oscillation maximum], which can be indeed fully characterized by the deformation of the supersolid structure discussed previously, affecting the amplitude and the spacing along the axial direction.

Instead, the case of the trap  $V_D$  presents a distinctive behavior associated with the emergence of a characteristic pattern in the background density distribution. This is visible in the top panels of Fig. 7 (middle and bottom rows). Remarkably, this pattern is reminiscent of the triangular lattice structure expected for 2D supersolids [37–40] (see also the discussion in Ref. [21]). We find that the corresponding transverse excitation mode (shown in the inset) is characterized by a relatively high frequency,  $\nu_{\perp} \simeq 60$  Hz, which couples with the axial breathing modes. This accounts for the “fast” oscillations that are visible in the continuous line at  $v_a = 0.05 a_0/\text{ms}$  in Fig. 7. As a matter of fact, a clean sinusoidal fit (with two or even three frequencies) is not possible in this case.

Finally, let us consider the excitation produced by the ramps in the opposite direction, when the system is driven into the SF phase. In this case we find that the condensate oscillations are dominated by a single excitation mode, namely, the axial breathing mode of a dipolar condensate discussed previously (see Fig. 8). This holds for both trap configurations,  $V_C$  and  $V_D$ . The corresponding frequency is expected to be slightly below the mean-field solution for the breathing mode frequency of a superfluid without dipolar interactions,  $\omega = \sqrt{5/2}\omega_x$  [46] (see again Ref. [12]). In particular, we find  $(\nu/\nu_x)_C \simeq 1.51$  ( $\epsilon_{dd}^C = 1.35$ ) and  $(\nu/\nu_x)_D \simeq 1.47$  ( $\epsilon_{dd}^D = 1.37$ ).

## V. CONCLUSIONS

We have presented a theoretical discussion—within the framework of the extended Gross-Pitaevskii theory including Lee-Huang-Yang quantum corrections—of the superfluid-supersolid transition of an elongated dipolar condensate as reported in the recent experiment by Biagioni *et al.* [21]. We have considered both trapping potentials employed in the experiment, providing a characterization of the equilibrium and

dynamical properties of the system as a function of the inter-particle scattering length, which is the parameter that is varied experimentally for driving the transition. Although both traps display a one row supersolid (for  $a_s < a_s^c$ ), already at the level of the ground state the two traps present a distinctive behavior. For a sufficiently strong transverse confinement (the trap  $V_C$ ) the SF-SS transition has a smooth continuous character, as it is expected for (quasi) 1D systems, with the superfluid and the supersolid states morphing continuously one into the other, as well as their energies. Instead, in the case of the potential  $V_D$ , which is characterized by a weaker transverse confinement, the transition clearly exhibits a discontinuous jump in the first derivative of the energy with respect to the  $s$ -wave scattering length, as it is expected for trapped supersolids with 2D lattice structures [37–40]. These properties reflect in the collective oscillations of the system, when the scattering length is dynamically ramped across the transition, from one phase to the other. In particular, we find that when the system is driven quasiadiabatically into the superfluid phase the system performs clean axial breathing oscillations, in both traps. In the opposite direction, the situation is quite different: in the trap  $V_C$  the excitation dynamics is still dominated by the doubling of the axial breathing modes, whereas when the transition becomes discontinuous, in the trap  $V_D$ , the collective excitations of the supersolid display a coupling with the transverse modes, signaling the onset of a dimensional crossover. These findings provide further insights on the experimental results reported in Ref. [21].

## ACKNOWLEDGMENTS

We thank G. Modugno, L. Tanzi, C. Gabbanini, and A. Fioretti from the Pisa-Florence Dysprosium laboratory for support and useful discussions. This work was supported by Grant No. PGC2018-101355-B-I00 funded by MCIN/AEI/10.13039/501100011033 and by “ERDF A way of making Europe”, by the Basque Government through Grant No. IT1470-22, by the QuantERA grant MAQS, and by Consiglio Nazionale delle Ricerche-Istituto Nazionale di Ottica (CNR-INO).

- 
- [1] E. P. Gross, Hydrodynamics of a superfluid condensate, *J. Math. Phys.* **4**, 195 (1963).
  - [2] L. Pitaevskii and S. Stringari, *Bose-Einstein Condensation and Superfluidity* (Oxford University, New York, 2016), Vol. 164.
  - [3] E. P. Gross, Unified theory of interacting bosons, *Phys. Rev.* **106**, 161 (1957).
  - [4] D. Kirzhnits and Y. A. Nepomnyashchii, Coherent crystallization of quantum liquid, *Sov. Phys. JETP* **32**, 1191 (1971).
  - [5] M. Boninsegni and N. V. Prokofev, Colloquium: Supersolids: What and where are they?, *Rev. Mod. Phys.* **84**, 759 (2012).
  - [6] V. I. Yukalov, Saga of superfluid solids, *Physics* **2**, 49 (2009).
  - [7] A. J. Leggett, Can a Solid Be “Superfluid”? *Phys. Rev. Lett.* **25**, 1543 (1970).
  - [8] G. Chester, Speculations on Bose-Einstein condensation and quantum crystals, *Phys. Rev. A* **2**, 256 (1970).
  - [9] L. Tanzi, E. Lucioni, F. Famà, J. Catani, A. Fioretti, C. Gabbanini, R. N. Bisset, L. Santos, and G. Modugno, Observation of a Dipolar Quantum Gas with Metastable Supersolid Properties, *Phys. Rev. Lett.* **122**, 130405 (2019).
  - [10] F. Böttcher, J.-N. Schmidt, M. Wenzel, J. Hertkorn, M. Guo, T. Langen, and T. Pfau, Transient Supersolid Properties in an Array of Dipolar Quantum Droplets, *Phys. Rev. X* **9**, 011051 (2019).
  - [11] L. Chomaz, D. Petter, P. Ilzhöfer, G. Natale, A. Trautmann, C. Politi, G. Durastante, R. M. W. van Bijnen, A. Patscheider, M. Sohmen, M. J. Mark, and F. Ferlaino, Long-Lived and Transient Supersolid Behaviors in Dipolar Quantum Gases, *Phys. Rev. X* **9**, 021012 (2019).
  - [12] L. Tanzi, S. M. Rocuzzo, E. Lucioni, F. Famà, A. Fioretti, C. Gabbanini, G. Modugno, A. Recati, and S. Stringari, Supersolid symmetry breaking from compressional oscillations in a dipolar quantum gas, *Nature (London)* **574**, 382 (2019).
  - [13] M. Guo, F. Böttcher, J. Hertkorn, J.-N. Schmidt, M. Wenzel, H. P. Büchler, T. Langen, and T. Pfau, The low-energy

- Goldstone mode in a trapped dipolar supersolid, *Nature (London)* **574**, 386 (2019).
- [14] G. Natale, R. M. W. van Bijnen, A. Patscheider, D. Petter, M. J. Mark, L. Chomaz, and F. Ferlaino, Excitation Spectrum of a Trapped Dipolar Supersolid and Its Experimental Evidence, *Phys. Rev. Lett.* **123**, 050402 (2019).
- [15] L. Tanzi, J. G. Maloberti, G. Biagioni, A. Fioretti, C. Gabbanini, and G. Modugno, Evidence of superfluidity in a dipolar supersolid from nonclassical rotational inertia, *Science* **371**, 1162 (2021).
- [16] M. A. Norcia, C. Politi, L. Klaus, E. Poli, M. Sohmen, M. J. Mark, R. N. Bisset, L. Santos, and F. Ferlaino, Two-dimensional supersolidity in a dipolar quantum gas, *Nature (London)* **596**, 357 (2021).
- [17] M. Sohmen, C. Politi, L. Klaus, L. Chomaz, M. J. Mark, M. A. Norcia, and F. Ferlaino, Birth, Life, and Death of a Dipolar Supersolid, *Phys. Rev. Lett.* **126**, 233401 (2021).
- [18] J. Léonard, A. Morales, P. Zupancic, T. Esslinger, and T. Donner, Supersolid formation in a quantum gas breaking a continuous translational symmetry, *Nature (London)* **543**, 87 (2017).
- [19] J.-R. Li, J. Lee, W. Huang, S. Burchesky, B. Shteynas, F. Ç. Top, A. O. Jamison, and W. Ketterle, A stripe phase with supersolid properties in spin-orbit-coupled Bose-Einstein condensates, *Nature (London)* **543**, 91 (2017).
- [20] S. C. Schuster, P. Wolf, S. Ostermann, S. Slama, and C. Zimmermann, Supersolid Properties of a Bose-Einstein Condensate in a Ring Resonator, *Phys. Rev. Lett.* **124**, 143602 (2020).
- [21] G. Biagioni, N. Antolini, A. Alaña, M. Modugno, A. Fioretti, C. Gabbanini, L. Tanzi, and G. Modugno, Dimensional Crossover in the Superfluid-Supersolid Quantum Phase Transition, *Phys. Rev. X* **12**, 021019 (2022).
- [22] N. Sepúlveda, C. Josserand, and S. Rica, Nonclassical rotational inertia fraction in a one-dimensional model of a supersolid, *Phys. Rev. B* **77**, 054513 (2008).
- [23] D. Petter, A. Patscheider, G. Natale, M. J. Mark, M. A. Baranov, R. van Bijnen, S. M. Rocuzzo, A. Recati, B. Blakie, D. Baillie, L. Chomaz, and F. Ferlaino, Bragg scattering of an ultracold dipolar gas across the phase transition from Bose-Einstein condensate to supersolid in the free-particle regime, *Phys. Rev. A* **104**, L011302 (2021).
- [24] Y. Pomeau and S. Rica, Dynamics of a Model of Supersolid, *Phys. Rev. Lett.* **72**, 2426 (1994).
- [25] T. Macrì, F. Maucher, F. Cinti, and T. Pohl, Elementary excitations of ultracold soft-core bosons across the superfluid-supersolid phase transition, *Phys. Rev. A* **87**, 061602(R) (2013).
- [26] Z.-K. Lu, Y. Li, D. S. Petrov, and G. V. Shlyapnikov, Stable Dilute Supersolid of Two-Dimensional Dipolar Bosons, *Phys. Rev. Lett.* **115**, 075303 (2015).
- [27] F. Dalfovo, S. Giorgini, L. P. Pitaevskii, and S. Stringari, Theory of Bose-Einstein condensation in trapped gases, *Rev. Mod. Phys.* **71**, 463 (1999).
- [28] S. Ronen, D. C. E. Bortolotti, and J. L. Bohn, Bogoliubov modes of a dipolar condensate in a cylindrical trap, *Phys. Rev. A* **74**, 013623 (2006).
- [29] F. Wächtler and L. Santos, Ground-state properties and elementary excitations of quantum droplets in dipolar Bose-Einstein condensates, *Phys. Rev. A* **94**, 043618 (2016).
- [30] M. Schmitt, M. Wenzel, F. Böttcher, I. Ferrier-Barbut, and T. Pfau, Self-bound droplets of a dilute magnetic quantum liquid, *Nature (London)* **539**, 259 (2016).
- [31] W. H. Press, S. A. Teukolsky, W. T. Vetterling, and B. P. Flannery, *Numerical Recipes: The Art of Scientific Computing*, 3rd ed. (Cambridge University, New York, 2007).
- [32] Modugno, M., Pricoupenko, L., and Castin, Y., Bose-Einstein condensates with a bent vortex in rotating traps, *Eur. Phys. J. D* **22**, 235 (2003).
- [33] C. Politi, A. Trautmann, P. Ilzhöfer, G. Durastante, M. J. Mark, M. Modugno, and F. Ferlaino, Interspecies interactions in an ultracold dipolar mixture, *Phys. Rev. A* **105**, 023304 (2022).
- [34] The full size of the computational box is  $54 \times 18 \times 18 \mu\text{m}$ . The typical number of grid points in the numerical simulations is  $192 \times 64 \times 64$ .
- [35] Numerically, these two states are obtained by using different initial trial wave functions, exploiting the fact that the conjugate gradient algorithm used in the minimization procedure is sensitive to the initial conditions.
- [36] Without an external trapping potential, a change of the lattice phase costs zero energy, therefore in the infinite system the phase of the supersolid lattice is undefined. This is no longer the case in trapped systems, where among all the possible phases only two minimize the cost in trapping energy. These two states correspond to the two almost degenerate configurations, characterized by either a maximum or a minimum at the center of the trap.
- [37] Y.-C. Zhang, F. Maucher, and T. Pohl, Supersolidity around a Critical Point in Dipolar Bose-Einstein Condensates, *Phys. Rev. Lett.* **123**, 015301 (2019).
- [38] Y.-C. Zhang, T. Pohl, and F. Maucher, Phases of supersolids in confined dipolar Bose-Einstein condensates, *Phys. Rev. A* **104**, 013310 (2021).
- [39] J. Hertkorn, J.-N. Schmidt, M. Guo, F. Böttcher, K. S. H. Ng, S. D. Graham, P. Uerlings, H. P. Büchler, T. Langen, M. Zwerlein, and T. Pfau, Supersolidity in Two-Dimensional Trapped Dipolar Droplet Arrays, *Phys. Rev. Lett.* **127**, 155301 (2021).
- [40] T. Bland, E. Poli, C. Politi, L. Klaus, M. A. Norcia, F. Ferlaino, L. Santos, and R. N. Bisset, Two-Dimensional Supersolid Formation in Dipolar Condensates, *Phys. Rev. Lett.* **128**, 195302 (2022).
- [41] While those dissipation effects could be easily implemented in the simulations, we refrain from doing so for the sake of clarity and to better identify the underlying dynamics.
- [42] The GP equation is solved by means of a FFT split-step method (see, e.g., Ref. [47]).
- [43] A similar argument holds also in the SS phase once the supersolid has been formed.
- [44] A. Gallemí, S. M. Rocuzzo, S. Stringari, and A. Recati, Quantized vortices in dipolar supersolid Bose-Einstein-condensed gases, *Phys. Rev. A* **102**, 023322 (2020).
- [45] A direct quantitative comparison with Ref. [12] is not possible because the actual values of the frequencies depend on the parameters of the system, which are different.
- [46] S. Stringari, Collective Excitations of a Trapped Bose-Condensed Gas, *Phys. Rev. Lett.* **77**, 2360 (1996).
- [47] B. Jackson, J. F. McCann, and C. S. Adams, Output coupling and flow of a dilute Bose-Einstein condensate, *J. Phys. B* **31**, 4489 (1998).